



# Far-field analysis of the Malyuzhinets solution for plane and surface waves diffraction by an impedance wedge

A.N. Norris <sup>a,\*</sup>, A.V. Osipov<sup>b,1</sup>

Department of Mechanical and Aerospace Engineering, Rutgers University, 98 Brett Road, Piscataway, NJ 08854-8058, USA
 Institute of Radiophysics, The St. Petersburg State University, Uljanovskaja 1-1, Petrodvorets 198904, Russia

Received 20 December 1996; received in revised form 13 July 1998; accepted 17 September 1998

#### **Abstract**

The basic problem of determining the far-field scattered from the edge of a wedge of exterior angle  $2\Phi$  with arbitrary impedance conditions on either face is considered. An accurate solution in the form of a Sommerfeld integral obtained by Malyuzhinets is evaluated for  $kr\gg 1$ . A fairly complete discussion of the far-field response is provided, including uniform and non-uniform asymptotic approximations. The far-field is split into edge-diffracted, surface, and geometrical optics waves, including multiply reflected components. The edge-diffracted field is defined by the diffraction coefficient, which we show has a simple factorisation:  $D=u_0(\phi)u_0(\phi_0)F_{\Phi}(\phi,\phi_0)$ , where  $\phi$  and  $\phi_0$  are the source and observation directions,  $u_0(\phi)$  is the value of the wave function at the edge for a plane wave of unit amplitude incident from the direction  $\phi$ , and  $F_{\Phi}(\phi,\phi_0)$  involves only trigonometric functions. We demonstrate that the monostatic tip diffraction from a wedge of arbitrary angle can be made to vanish by appropriate choice of the surface impedance. The unique value of impedance is always real, and an explicit formula is given for its evaluation. New results are presented for the reflection and transmission of surface waves on an impedance wedge, including simple approximations for an internal wedge with small  $\Phi$ . Finally, a complete uniform description of the far-field is given in the format of the Uniform Asymptotic Theory of Diffraction. ©1999 Elsevier Science B.V. All rights reserved.

#### 1. Introduction

A two-dimensional time-harmonic scalar wave field  $u(r, \phi)$  is excited in a wedge-shaped region  $0 < r < \infty$ ,  $|\phi| < \phi$ , Fig. 1, by a plane wave incident from the direction  $\phi_0$ ,

$$u_{\rm inc}(r,\phi) = U_0 \exp[-ikr\cos(\phi - \phi_0)]. \tag{1}$$

Here  $k = \omega/c$  and c is the wave speed, and the time dependance factor  $e^{-i\omega t}$  is 1 filomitted throughout. The field

 $<sup>\</sup>hbox{$^*$ Corresponding author. E-mail: norris@norris.rutgers.edu}\\$ 

<sup>&</sup>lt;sup>1</sup> Present address: German Aerospace Center, DLR Institute of Radio Frequency Technology, PO Box 1116, D-82230 Wessling, Germany. E-mail: aosipov@ieee.org

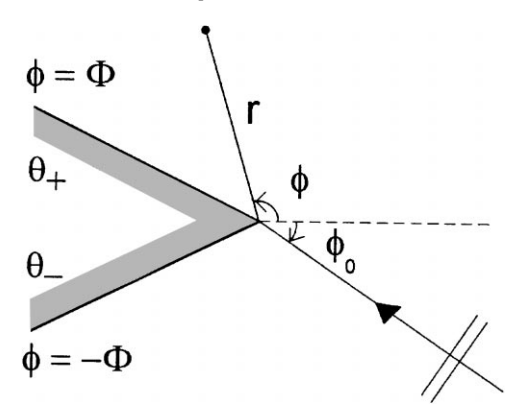


Fig. 1. The geometry.

satisfies the Helmholtz equation

$$\frac{\partial^2 u}{\partial r^2} + \frac{1}{r} \frac{\partial u}{\partial r} + \frac{1}{r^2} \frac{\partial^2 u}{\partial \phi^2} + k^2 u = 0, \tag{2}$$

within the wedge-shaped region, and impedance boundary conditions of the form

$$\frac{1}{r}\frac{\partial u}{\partial \phi} \mp ik\sin\theta_{\pm}u = 0,\tag{3}$$

on the wedge faces  $\phi = \pm \Phi$ . The complex-valued angles  $\theta_{\pm}$  are related to normalised surface impedances of the wedge faces (the actual surface impedances are  $Z_{\pm} = \rho c/\sin\theta_{\pm}$ ,  $\rho c$  being the acoustic impedance, so that  $\sin\theta_{\pm}$  are really the normalised surface admittances, the inverse of impedance). For any physically passive boundary, which is free of field sources, simple energy considerations imply that  $0 < \text{Re } \theta_{\pm} \le \pi/2$ , whereas  $\text{Im } \theta_{\pm}$  can be arbitrary.

The function  $u(r, \phi)$  is a potential function which, depending on the sort of wave motion we are dealing with, represents a certain physical quantity, e.g., the sound pressure or a component of the electromagnetic field. As such it should meet specific conditions at the edge of the wedge so as to guarantee physically correct behaviour of the wave field there. These edge conditions may be written as

$$|u(0,\phi)| = C, \quad \lim_{r \to 0} \left| r \frac{\partial u}{\partial r} \right| = 0, \quad \lim_{r \to 0} \left| \frac{\partial u}{\partial \phi} \right| = 0,$$
 (4)

with C bounded and independent of  $\phi$  [1].

Far from the edge as  $kr \to +\infty$  the solution should recover the incident wave (1) and be free of any non-physical contributions. The corresponding condition may be expressed as

$$\lim_{r \to \infty} |u(r,\phi) - u_{\mathbf{g}}(r,\phi)| = 0, \quad \text{Im } k > 0,$$
(5)

where  $u_g(r,\phi)$  denotes the geometrical optics part of the field. The condition (5), or the so-called extinction condition (see [1,2]), extends the commonly used radiation conditions to the case of a plane wave illuminating scattering boundaries of infinite extent, by accounting for reflections of the incidence wave which are also incoming waves. The requirement Im k > 0 in (5), implying that the medium filling the wedge-shaped domain has some absorption, arbitrarily small at least, is necessary to exclude contributions of the form  $\exp(-ikr)/\sqrt{kr}$ , a forbidden counterpart of the edge diffracted field.

In order to include in our analysis a non-uniform excitation from an incoming surface wave we assume that  $\phi_0$  can be a complex number with an arbitrary imaginary part and with real part satisfying the relation  $-\Phi < \operatorname{Re} \phi_0 < \Phi$ .

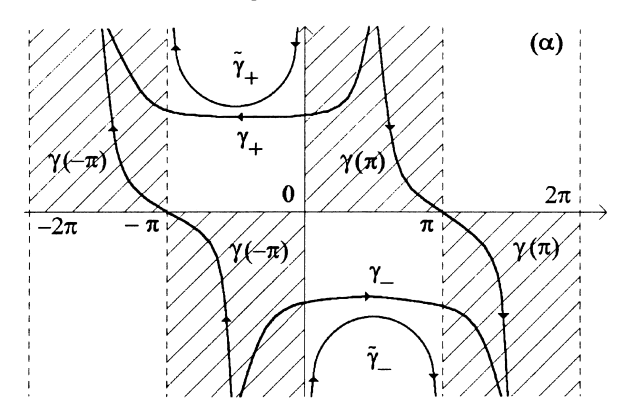


Fig. 2. The integration contours of the Sommerfeld integral.

In particular, putting  $\phi_0 = \Phi - \theta_+$  with Im  $\theta_+ < 0$  in (1) gives a surface wave travelling along the upper face of the wedge towards its edge. Analogously, the substitution  $\phi_0 = -\Phi + \theta_-$  with Im  $\theta_- < 0$  transforms the excitation (1) into an incoming surface wave propagating over the lower face of the wedge.

An elegant solution to the diffraction problem defined by Eqs. (1)–(5) has been deduced by Malyuzhinets in his Doctor of Science Dissertation [1], and later described in a series of papers culminating in the concise solution outlined in his 1958 paper [3]. The method of solution is discussed in detail in our companion review paper [4], which contains all the pertinent references. In summary: the solution is expressed as a Sommerfeld integral over the contour  $\gamma = \gamma_+ \cup \gamma_-$ ,

$$u(r,\phi) = \frac{1}{2\pi i} \int_{\gamma} e^{-ikr\cos\alpha} S(\alpha + \phi) d\alpha, \tag{6}$$

where  $\gamma_+$  is a loop in the upper half of the complex  $\alpha$ -plane, beginning at  $\pi/2 + i\infty$ , ending at  $-3\pi/2 + i\infty$ , with Im  $\alpha$  lying above an arbitrary minimum, such that no singularities of the integrand occur within  $\gamma_+$  for all  $|\phi| \leq \Phi$ . The contour  $\gamma_-$  is the image of  $\gamma_+$  under inversion about the origin  $\alpha = 0$  (Fig. 2).

The transform function

$$S(\alpha) = U_0 \frac{\Psi(\alpha)}{\Psi(\phi_0)} \sigma(\alpha) \tag{7}$$

is expressed in terms of trigonometric functions

$$\sigma(\alpha) = \frac{\nu \cos(\nu \phi_0)}{\sin(\nu \alpha) - \sin(\nu \phi_0)}, \quad \nu = \frac{\pi}{2\Phi},$$
(8)

and a transcendental function

$$\Psi(\alpha) = \psi_{\Phi} \left( \alpha + \Phi + \frac{\pi}{2} - \theta_{+} \right) \psi_{\Phi} \left( \alpha + \Phi - \frac{\pi}{2} + \theta_{+} \right) \times \psi_{\Phi} \left( \alpha - \Phi - \frac{\pi}{2} + \theta_{-} \right) \psi_{\Phi} \left( \alpha - \Phi + \frac{\pi}{2} - \theta_{-} \right). \tag{9}$$

The latter is a particular solution to the system of difference equations

$$\frac{\Psi(\alpha \pm \Phi)}{\Psi(-\alpha \pm \Phi)} = \frac{-\sin\alpha \pm \sin\theta_{\pm}}{\sin\alpha \pm \sin\theta_{\pm}},\tag{10}$$

and can be expressed in terms of a special function  $\psi_{\Phi}(\alpha)$  introduced by Malyuzhinets [3]. Alternative but equivalent solutions to the impedance wedge diffraction problem were later derived independently by Williams [5] and Senior [6].

The impedance wedge geometry is one of the canonical shapes of high-frequency diffraction theory. By evaluating the integral (6) for  $kr \gg 1$ , one may obtain asymptotic representations of the field scattered from an edge in an impedance surface [3,7–10]. These can then be incorporated into various versions of the high-frequency diffraction theory, including the geometrical theory of diffraction (GTD, [11]) and its uniform formulations – the uniform asymptotic theory of diffraction (UAT, [12–14]), and the uniform geometrical theory of diffraction (UTD, [15]). Accurate solutions to the canonical problems are also used in applied versions of the high-frequency diffraction theory, aimed at solving engineering problems, like the physical theory of diffraction (PTD, [16]) and other techniques utilising the concepts of incremental length diffraction coefficients [17–19], equivalent edge currents [20–23], and elementary edge waves [24,25].

This paper provides a complete high-frequency analysis of the Malyuzhinets solution. We subsequently analyse various components forming the far field response. Wherever possible the accurate formulas for the field components are supplemented with simple approximations in order to facilitate quantitative understanding of the far-field behaviour. In Section 2 the response from a wedge with locally reacting impedance boundary conditions on each face is naturally split into geometrical optics, surface, and diffracted wave components. We demonstrate in Section 2.1 that the geometrical optics part involves reflections from the faces and may be described using reflection coefficients for the separate faces combined with ray tracing. Multiply reflected rays occur in the case of an internal wedge, when  $\Phi < \pi/2$ .

Section 2.2 deals with the surface waves that arise from diffraction of the incident field at the edge. If  $\Phi < \pi/4$ , these may also include multiply reflected components. Both plane and surface wave excitations are considered. The equation of energy balance between incident, reflected and transmitted surface waves and the edge diffracted volume wave is presented and the dependence of each component on the wedge angle  $\Phi$  is numerically estimated. We also give simple but surprisingly accurate approximations for the surface wave transmission and reflection coefficients.

The edge diffracted waves, on the other hand, are generally more difficult to handle, because their amplitude and phase depend upon complicated and non-intuitive functions. The diffracted field is particularly important in shadow zones where no direct or multiply reflected wavefronts occur. Section 2.3 offers a simple way of viewing the diffracted response, using only trigonometric functions as far as possible. We show that the edge diffraction coefficient can be represented in a particularly simple and physically revealing form. Some consequences of the new form are explored and discussed. Specifically, we analyse backscattering from an impedance wedge and demonstrate that at particular observation angles the monostatic echowidth of the wedge can be made to vanish by appropriate choice of its face impedances. The unique value of impedance is always real, and an explicit formula is given in Section 2.3 for its evaluation.

The paper ends with a complete set of uniform asymptotic far-field expressions for the total field diffracted by an impedance wedge (Section 3). In this part of our paper we follow an elegant approach described in [14] for a particular case of perfectly reflecting wedge boundaries. This leads directly to asymptotic expansions of the far-field as series in inverse powers of kr, without having to evaluate the Malyuzhinets integral (6) when the poles of its integrand approach the saddle points, or by first solving an associated problem for pulse excitation in the time domain, as done in [26].

The asymptotic expressions of Section 3 are deduced in the format of UAT. There are alternative formats for expressing the fields diffracted by wedges in a uniform manner, e.g., those of UTD. They are known to correspond to the use of different procedures for evaluating integrals over steepest descent paths in the case of a pole approaching a saddle point [27]. This produces superficially different asymptotic representations of the far-field, which may utilise functions other than the Fresnel integral to describe the field in transition regions (see, e.g., [7,8,28]). However, they are obviously equivalent formulations as long as accurate techniques are employed for the asymptotic evaluation of the solution (for further discussion of the subject, see, e.g., [27]).

#### 2. The structure of the far-field

The far-field representation of a solution expressed as the Sommerfeld integral (6) is constructed by deforming the integration contour  $\gamma = \gamma_+ \cup \gamma_-$  into a pair of contours  $\gamma(\pm \pi)$  (Fig. 2) which are the steepest descent paths (SDPs) associated with the exponent factor  $\exp(-ikr\cos\alpha)$  [3]. The SDPs are

$$\gamma(\pm \pi) = \{\alpha : \operatorname{Re} \alpha = \pm \pi - \operatorname{gd}(\operatorname{Im} \alpha)\},\tag{11}$$

with  $gd(x) = -\pi/2 + 2 \arctan(e^x)$ . This produces a representation of the form

$$u(r,\phi) = u_{\rm g}(r,\phi) + u_{\rm d}(r,\phi) + u_{\rm S}(r,\phi),$$
 (12)

where the contribution from integration over the SDPs is

$$u_{\rm d}(r,\phi) = \frac{1}{2\pi i} \int_{\gamma(\pi)\cup\gamma(-\pi)} e^{-ikr\cos\alpha} S(\alpha+\phi) \,\mathrm{d}\alpha. \tag{13}$$

The other terms in (12) arise from residues at poles of the transform function  $S(\alpha)$  captured by the contour deformation. Such poles are located in the region  $\Pi^{RES}$  enclosed by the SDPs  $\gamma(\pm \pi)$  to its left and right and by the Sommerfeld contours  $\gamma_{\pm}$  at its top and bottom.

It is interesting to note that because of the specific structure of the integration contours  $\gamma(\pm \pi)$  which are offset by  $2\pi$  from each other and are taken in opposite directions (Fig. 2), the integral in (13) cancels implying that

$$u_{\rm d}(r,\phi)$$
 vanishes everywhere if  $S(\alpha)$  is  $2\pi$ -periodic.

The conditions for such periodicity have been formulated in our previous paper [4]. They require that the wedge semi-angle  $\Phi$  must be a rational fraction of  $\pi$ , i.e.,  $\Phi = \pi/(4m)$  with m = 1, 2, 3, ... In the case of identical faces of the wedge when  $\theta_+ = \theta_-$ ,  $S(\alpha)$  is  $2\pi$ -periodic for a broader variety of angles defined by the relations  $\Phi = \pi/(2q)$  with q being any integer. Thus, in these cases the wave field  $u(r, \phi)$  diffracted by an impedance wedge can be expressed without integration as a finite number of contributions all occurring from residues at the poles residing within  $\Pi^{RES}$ .

Each component of the representation (12) has a clear physical meaning, in accord with the simple fact that far from the edge of the wedge the total wave field should comprise the incoming plane wave plus a scattered wave which in turn can be split into reflected ray-optic contributions, surface waves associated with the impedance faces of the wedge, and a diffracted wave emanating from its edge. A successive discussion of these terms now follows.

## 2.1. The geometrical optics field

Evaluating the residues at poles of  $\sigma(\alpha + \phi)$  yields the expression of the form [3]

$$u_{g}(r,\phi) = U_{0} \sum_{n=-\infty}^{+\infty} (-1)^{n} H(\pi - |\delta_{n}(\phi,\phi_{0},\Phi)|) \frac{\Psi[(-1)^{n}\phi_{0} + 2n\Phi]}{\Psi(\phi_{0})} e^{-ikr\cos[\phi - (-1)^{n}\phi_{0} - 2n\Phi]},$$
(14)

where

$$\delta_n(\phi, \phi_0, \Phi) = \phi - 2n\Phi - (-1)^n [gd(Im \phi_0) + Re \phi_0],$$

and H(x) = 1 if x > 0, and H(x) = 0, if x < 0. The step functions in (14) are clearly non-zero only for those poles of  $\sigma(\alpha + \phi)$  that are located in  $\Pi^{RES}$ . This means that the total number of contributions to  $u_g(r, \phi)$  is always finite, although it may be rather large for small  $\Phi$ , because this latter parameter determines the spacing between the poles. The smaller the  $\Phi$ , the more members are involved in (14).

The formula (14) allows for complex values of  $\phi_0$  and includes therefore the case of non-uniform excitation. If the incoming field is a plane wave, then  $\phi_0$  is real and  $\delta_n(\phi, \phi_0, \Phi)$  simplifies to  $\phi - 2n\Phi - (-1)^n\phi_0$ .

Consider the physical interpretation of (14). The phase factors in (14) coincide with those appearing in the geometrical optics representations of fields scattered by wedges with perfectly reflecting boundaries [29,30], and clearly correspond to multiply reflected plane waves. In contrast, the amplitude factors in (14) appear to be more complex to interpret, since in the framework of Malyuzhinets theory they are initially given by ratios of the special functions  $\Psi(\alpha)$ . However, these ratios can be reduced to products of conventional planar reflection coefficients [9,31,32]. By substituting  $\alpha \to -\phi_0 \pm \Phi$  in Eqs. (10) satisfied by  $\Psi(\alpha)$ , one gets the relations

$$\frac{\Psi(\pm 2\Phi - \phi_0)}{\Psi(\phi_0)} = -R_{\pm}(\Phi \mp \phi_0),\tag{15}$$

where  $R_{\pm}(\chi) = (\sin \chi - \sin \theta_{\pm})/(\sin \chi + \sin \theta_{\pm})$  is the reflection coefficient for a plane wave incident at angle  $\chi$  upon a flat impedance surface. By repeatedly using the relations (15), each ratio of the auxiliary functions in (14) is reduced to a product of the reflection coefficients of different arguments, according to the identities:

$$\frac{\Psi(\alpha + 4n\Phi)}{\Psi(\alpha)} = \prod_{j=1}^{n} R_{-}(\alpha - 3\Phi + 4j\Phi)R_{+}(\alpha - \Phi + 4j\Phi), \quad n \ge 1,$$

$$\frac{\Psi(\alpha + 4n\Phi)}{\Psi(\alpha)} = 1, \quad n = 0,$$

$$\frac{\Psi(\alpha + 4n\Phi)}{\Psi(\alpha)} = \prod_{j=1}^{n} R_{+}(-\alpha - 3\Phi + 4j\Phi)R_{-}(-\alpha - \Phi + 4j\Phi), \quad n \le -1,$$

$$\frac{\Psi(-\alpha + 2\Phi + 4n\Phi)}{\Psi(\alpha)} = -R_{+}(\Phi - \alpha) \prod_{j=1}^{n} R_{-}(-\alpha - \Phi + 4j\Phi)R_{+}(-\alpha + \Phi + 4j\Phi), \quad n \ge 0,$$

$$\frac{\Psi(-\alpha + 2\Phi + 4n\Phi)}{\Psi(\alpha)} = -R_{-}(\Phi + \alpha) \prod_{j=1}^{n-1} R_{+}(\alpha - \Phi + 4j\Phi)R_{-}(\alpha + \Phi + 4j\Phi), \quad n \le -1,$$
(17)

where  $\alpha$  is an arbitrary complex parameter, while n is an arbitrary integer.

Based upon (16) and (17) we conclude that  $u_g(r, \phi)$  is the geometrical optics part of the wave field. Each term of (14) is a plane wave reflected by the wedge faces, except for the term with n=0 which is an incident wave. In the case of an external, or acute, wedge implying that  $\Phi > \pi/2$ , there always exist only three non-zero contributions to (14), relevant to the direct and singly reflected waves. For small  $\Phi$  (a narrow wedge-shaped region or an internal or obtuse wedge), further contributions may appear, representing multiply reflected images of the incident wave.

#### 2.2. The surface waves

Next, we consider the contributions to (12) from the function  $\Psi(\alpha + \phi)$ . Note that  $\Psi(\alpha)$  is a meromorphic function of its argument [3,4], and its poles are simply those of the four Malyuzhinets functions appearing in (9). Since  $\psi_{\Phi}(\alpha)$  has its poles at  $\alpha = \pm \beta_{pq}$  where  $\beta_{pq} = (\pi/2)(2q-1) + 2\Phi(2p-1)$  with  $p=1,2,3,\ldots$ , an arbitrary positive integer and  $q=2,4,6,\ldots$ , even and positive [3], the following poles of  $\Psi(\alpha + \phi)$  may fall within  $\Pi^{RES}$  and may be captured 1fil in the course of deformation of the Sommerfeld contours  $\gamma_{\pm}$  onto the

SDPs  $\gamma(\pm \pi)$ :

$$\alpha_{jm} = -\phi + (-3\Phi + \pi + \theta_{+} + 4m\Phi), \quad j = 1, \quad m = 1, 2, \dots$$

$$\alpha_{jm} = -\phi + (\Phi - \pi - \theta_{+} - 4m\Phi), \quad j = 2, \quad m = 1, 2, \dots$$

$$\alpha_{jm} = -\phi + (3\Phi - \pi - \theta_{-} - 4m\Phi), \quad j = 3, \quad m = 1, 2, \dots$$

$$\alpha_{jm} = -\phi + (-\Phi + \pi + \theta_{-} + 4m\Phi), \quad j = 4, \quad m = 1, 2, \dots$$
(18)

Here j labels the four families of poles of  $\Psi(\alpha + \phi)$ .

In accordance with the form of (18) the residue contributions to the total field (12) may be represented as

$$u_{s}(r,\phi) = \sum_{j=1}^{4} \sum_{m=1}^{M_{j}} u_{jm}(r,\phi), \tag{19}$$

where each member  $u_{jm}(r, \phi)$  arises from the pole  $\alpha = \alpha_{jm}$ , and  $M_j$  with j = 1, 2, 3, 4 are integers equal to the number of captured poles from the jth family. Their values are functions of the configuration parameters  $\theta_{\pm}$ ,  $\Phi$ , and  $\phi$ . Later we present explicit expressions for these quantities.

In the case of an external wedge,  $\Phi > \pi/2$ , only the poles with m = 1 and j = 1 or j = 3 can be crossed. This simplifies the representation (19) to

$$u_{s}(r,\phi) = u_{+}(r,\phi) + u_{-}(r,\phi),$$
 (20)

where

$$u_{\pm}(r,\phi) = U_0 A_{\pm}(\phi_0) H[\pm \phi - \Phi - \operatorname{Re}\theta_{\pm} - \operatorname{gd}(\operatorname{Im}\theta_{\pm}) \exp[ikr \cos(\Phi \mp \phi + \theta_{\pm})], \tag{21}$$

and

$$A_{\pm}(\phi_0) = -\frac{2\nu\cos(\nu\phi_0)\tan\theta_{\pm}}{\cos\left[\nu(\pi + \theta_{\pm})\right] \mp \sin(\nu\phi_0)} \frac{\Psi(\pm\Phi \mp \pi \mp \theta_{\pm})}{\Psi(\phi_0)}.$$
 (22)

The Heaviside step function H(x) in (21) accounts for the conditions required to capture the poles  $\alpha = \alpha_{11}$  and  $\alpha = \alpha_{31}$ . Notice that  $u_+(r,\phi)$  and  $u_-(r,\phi)$  vanish if  $\text{Im }\theta_+>0$  and  $\text{Im }\theta_->0$ , respectively, because the corresponding poles are not captured. This means that non-zero contributions to Eq. (20) may appear only when at least one of the conditions  $\text{Im }\theta_\pm<0$  is met.

With Im  $\theta_{\pm} < 0$  the expressions (21) describe a function that is concentrated near a corresponding boundary of the wedge, decaying exponentially when the observation point moves in the normal direction outwards from the face. These contributions also decrease as the distance r from the edge grows, except for the case of non-absorbing boundaries, Re  $\theta_{\pm} = 0$ , in which case the functions  $u_{\pm}(r, \pm \Phi)$  become purely oscillatory. It is obvious from the analysis of the phase factors in (21) that these contributions can be interpreted as surface waves excited by an incident wave at the edge of the wedge which then travel outwards from the edge along the faces. Note that the conditions for exciting these waves are exactly those for the excitation of a surface wave by a line source placed at a point r = 0 on an impedance plane, although the amplitude coefficients  $A_{\pm}(\phi_0)$  differ.

Note that in deriving the expression (22) it was necessary to evaluate the residues of the transform function  $S(\alpha)$  at poles of  $\Psi(\alpha)$ . In order to avoid the appearance of derivatives of special Malyuzhinets functions we have invoked the functional relations (10), thereby extracting the singularities in multiplicative factors which include only trigonometric functions and can be differentiated explicitly.

Next, by using the functional property [3]:

$$\psi_{\Phi}\left(\alpha + \frac{\pi}{2}\right)\psi_{\Phi}\left(\alpha - \frac{\pi}{2}\right) = \psi_{\Phi}^{2}\left(\frac{\pi}{2}\right)\cos\left(\frac{\pi\alpha}{4\Phi}\right),\tag{23}$$

one may express the functions  $\Psi(\pm\Phi\mp\pi\mp\theta_{\pm})$  in (22) through  $\Psi(\pm\Phi\mp\theta_{\pm})$ . The latter function always has its argument within the strip  $|\text{Re }\alpha| \leq \Phi$  where by construction the function  $\Psi(\alpha)$  is free of both zeros and poles [3,4]. This yields the formulas

$$A_{\pm}(\phi_0) = -2\nu \sin\left(\frac{\nu\pi}{2}\right) \psi_{\phi}^8 \left(\frac{\pi}{2}\right) \cos(\nu\phi_0) \tan\theta_{\pm} \sin(\nu\theta_{\pm})$$

$$\times \frac{\cos\left[(\nu/2)(\theta_+ + \theta_-)\right] \cos\left[(\nu/2)(\pi + \theta_{\pm} - \theta_{\mp})\right]}{\Psi(\phi_0)\Psi(\pm\Phi \mp \theta_+)\left\{\cos\left[\nu(\pi + \theta_+)\right] \mp \sin(\nu\phi_0)\right\}},$$
(24)

which can be advantageous for numerical purposes.

Alternatively, the surface wave amplitudes can be written succinctly in terms of the normalised edge field  $u_0$  which is defined by the formula

$$u_0(\phi) = \frac{u(0,\phi)}{U_0},\tag{25}$$

where  $u(0, \phi)$  is the tip value of the total field [3,4]:

$$\lim_{r \to 0} u(r, \phi) = U_0 \frac{v \cos(v\phi_0)}{\Psi(\phi_0)} \psi_{\phi}^4 \left(\frac{\pi}{2}\right). \tag{26}$$

By using Eqs. (25) and (26), one may rewrite (24) as follows:

$$A_{\pm}(\phi_0) = -\frac{2}{\nu} \sin\left(\frac{\nu\pi}{2}\right) \tan\theta_{\pm} \frac{\cos\left[(\nu/2)(\theta_+ + \theta_-)\right] \cos\left[(\nu/2)(\pi + \theta_{\pm} - \theta_{\mp})\right]}{\cos\left[\nu(\pi + \theta_{\pm})\right] \mp \sin(\nu\phi_0)} \times u_0(\phi_0) u_0(\pm\Phi \mp \theta_{\pm}). \tag{27}$$

This representation is remarkable in that it involves only trigonometric functions in addition to the edge fields. Similar property also holds for the edge diffracted field and is discussed in Section 2.3. As one might expect, one of the edge fields in (27) is evaluated for a complex angle of incidence, appropriate to a surface wave.

In the case of surface wave incidence, the total field is given by (12) with  $\phi_0 = \pm \Phi \mp \theta_{\pm}$ , and consists of the incident surface wave, the reflected and transmitted surface waves, and the edge diffracted wave. Correspondingly, the excitation coefficients  $A_{\pm}(\phi_0)$  become the reflection and transmission coefficients. These are  $r_{++} = A_{+}(\Phi - \theta_{+})$  and  $t_{+-} = A_{-}(\Phi - \theta_{+})$  if the excitation comes from the face  $\phi = \Phi$ , and  $r_{--} = A_{-}(-\Phi + \theta_{-})$  and  $t_{-+} = A_{+}(-\Phi + \theta_{-})$  if the incident surface wave comes from the lower face  $\phi = -\Phi$ . Simple algebraic manipulations of (24) yield

$$r_{\pm\pm} = \nu \psi_{\Phi}^{8} \left(\frac{\pi}{2}\right) \tan \theta_{\pm} \sin^{2}(\nu \theta_{\pm}) \frac{\cos \left[(\nu/2)(\theta_{+} + \theta_{-})\right] \cos \left[(\nu/2)(\pi + \theta_{\pm} - \theta_{\mp})\right]}{\Psi^{2}(\pm \Phi \mp \theta_{\pm}) \sin \left[(\nu/2)(2\theta_{\pm} + \pi)\right]},$$
(28)

for the surface wave reflection coefficients, and

$$t_{-+} = -\nu \psi_{\Phi}^{8} \left(\frac{\pi}{2}\right) \sin\left(\frac{\nu \pi}{2}\right) \frac{\tan \theta_{+} \sin(\nu \theta_{-}) \sin(\nu \theta_{+}) \cos\left[(\nu/2)(\theta_{+} + \theta_{-})\right]}{\Psi(\Phi - \theta_{+})\Psi(-\Phi + \theta_{-}) \cos\left[(\nu/2)(\pi + \theta_{+} + \theta_{-})\right]},\tag{29}$$

$$t_{+-} = -\nu \psi_{\Phi}^{8} \left(\frac{\pi}{2}\right) \sin\left(\frac{\nu \pi}{2}\right) \frac{\tan \theta_{-} \sin(\nu \theta_{+}) \sin(\nu \theta_{-}) \cos\left[\frac{\nu}{2}(\theta_{+} + \theta_{-})\right]}{\Psi(-\Phi + \theta_{-})\Psi(\Phi - \theta_{+}) \cos\left[\frac{\nu}{2}(\pi + \theta_{+} + \theta_{-})\right]},\tag{30}$$

for the transmissions coefficients. Note that  $t_{+-}$  cot  $\theta_- = t_{-+}$  cot  $\theta_+$ , which is exactly what is required by reciprocity because  $\tan\theta$  is the amplitude of the surface wave excited by a line source placed on an impedance plane with  $\theta$  being its Brewster angle. Also, in the case of equal impedances  $\theta_+ = \theta_-$ , one has  $r_{++} = r_{--}$  as expected from symmetry considerations. Finally, we note that in the limiting case of a flat impedance surface, which means that  $\theta_+ \to \theta_-$  and  $\Phi_- \to \pi/2$ , Eqs. (28)–(30) give  $r_{\pm\pm} \to 0$  and  $t_{\pm\mp} \to 1$ , as expected.

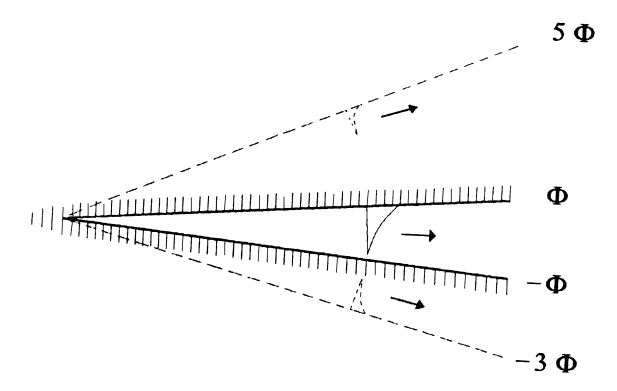


Fig. 3. Reflections of a surface wave in the Sommerfeld branched space.

When the wedge angle  $\Phi$  is less than  $\pi/4$ , further contributions with j=2 and j=4 may enter the representation (19). The tendency is that the smaller the wedge angle, the more the poles (18) can fall within the area  $\Pi^{RES}$  and be therefore crossed in the course of contour deformation. The number of captured poles can be explicitly expressed through the wedge parameters as follows:

$$M_{1} = 1 + \operatorname{entire} \left\{ \frac{1}{4\Phi} [-\operatorname{gd}(\operatorname{Im}\theta_{+}) - \operatorname{Re}\theta_{+} + \phi - \Phi] \right\},$$

$$M_{2} = \operatorname{entire} \left\{ \frac{1}{4\Phi} [-\operatorname{gd}(\operatorname{Im}\theta_{+}) - \operatorname{Re}\theta_{+} - \phi + \Phi] \right\},$$

$$M_{3} = 1 + \operatorname{entire} \left\{ \frac{1}{4\Phi} [-\operatorname{gd}(\operatorname{Im}\theta_{-}) - \operatorname{Re}\theta_{-} - \phi - \Phi] \right\},$$

$$M_{4} = \operatorname{entire} \left\{ \frac{1}{4\Phi} [-\operatorname{gd}(\operatorname{Im}\theta_{-}) - \operatorname{Re}\theta_{-} + \phi + \Phi] \right\},$$

$$(31)$$

where entire(x) denotes the biggest integer not greater than x.

The interested reader may find further formulas for contributions of such type as well as a more detailed discussion of this topic in [33]. Here we would like to just emphasize the physical interpretation of these contributions as multiply reflected surface waves. In order to make it apparent, consider in (19) the terms  $u_{jm}(r,\phi)$  with j=1 and  $m\geq 1$ . Their phase factors are  $\exp\{ikr\cos{[\Phi-\phi+\theta_++4\Phi(m-1)]}\}$  and that with m=1 describes a surface wave running in the direction  $\phi=\Phi$ . Consequently, the one with m=2 may be interpreted as a wave which propagates along the direction  $\phi=5\Phi$  on an attached sheet of a Sommerfeld branched space (Fig. 3) [34,35]. Thus, one may conclude that an mth term is a non-uniform wave directed to  $\phi=\Phi+4(m-1)\Phi$ . Though these directions are outside the physical region of space  $|\phi|\leq\Phi$ , such contributions appear in the field as a result of reflections of the initial surface wave between the wedge faces.

Analogously, the contributions with j=2 have  $\exp\{ikr\cos{[-3\Phi-\phi-\theta_+-4\Phi(m-1)]}\}$  as their phase factors. This allows us to associate them with another set of reflections of the same initial surface wave, propagating in the directions  $\phi=\Phi-4m\Phi$ , also outside the physical part of space (Fig. 3). If the initial surface wave propagates along the lower face of the wedge, the non-zero contributions to (19) are those with j=3 and j=4. They can similarly be interpreted as multiple reflections guided in the directions  $\phi=-\Phi\pm 4m\Phi$ .

In general, an incident surface wave, say the one incoming along the upper face  $\phi = \Phi$  of the wedge, converts at its edge into a cylindrical wave radiated outside the wedge, a reflected surface wave, propagating backward along the upper face, and a transmitted surface wave, travelling forward along the lower face  $\phi = -\Phi$ . In the case of a narrow internal wedge, the multiply reflected components may also occur. Assuming that the energy flux  $E_i$  of the incident surface wave is normalised to unity and there is no energy dissipation in the faces (Re  $\theta_+ = \text{Re }\theta_- = 0$ ),

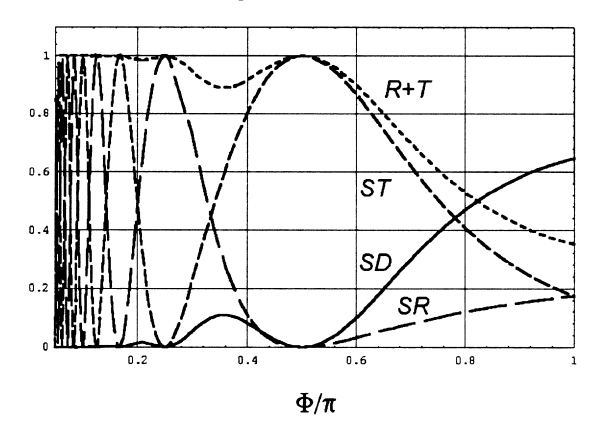


Fig. 4. The energy redistribution for surface wave excitation of an impedance wedge.

one finds the equation governing the energy balance for the conversion process in the far zone  $kr \gg 1$  to be as follows:

$$1 = |r_{++}|^2 + \tan \theta_+ \cot \theta_- |t_{+-}|^2 + \tan \theta_+ \frac{i}{\pi} \int_{-\Phi}^{\Phi} |D(\phi, \Phi - \theta_+)|^2 d\phi, \tag{32}$$

where the members in the right-hand side of the identity are the energy fluxes  $E_r$ ,  $E_t$ , and  $E_d$  associated with the reflected, transmitted, and radiated waves, respectively.  $D(\phi, \Phi - \theta_+)$  is the amplitude of the edge diffracted field when  $kr \to \infty$ . It is given by the diffraction coefficient  $D(\phi, \phi_0)$  with  $\phi_0 = \Phi - \theta_+$ , which is more precisely defined in Section 2.3. Note that the multiply reflected surface waves are not present in (32), since they vanish exponentially as  $kr \to \infty$  and, therefore, do not contribute to the far field.

Fig. 4 shows these energies as functions of the wedge angle  $\Phi$ , with the proviso that the impedances of the faces are the same and  $\theta_+ = \theta_- = -i$ . The curves "SR", "ST", and "SD" indicate the amounts of reflected surface, transmitted surface, and radiated spatial energies, respectively. The sum of the reflected and transmitted surface wave energies is the curve "R+T". The total of this latter and the radiated spatial energy equals unity, the energy of the incident surface wave.

For small values of  $\Phi$ , approximately  $\Phi < \pi/5$ , the values of  $E_{\rm r}$  and  $E_{\rm t}$  oscillate strongly, even though their sum  $E_{\rm s} = E_{\rm r} + E_{\rm t}$ , that is, the total energy flux associated with both the reflected and transmitted surface waves, remains a smooth function tending to unity as  $\Phi$  approaches zero. In fact, by explicitly making the approximation  $E_{\rm s} \equiv 1$ , the formulae for the reflection and transmission coefficients give simple but surprisingly accurate estimates  $E_{\rm r} \approx \cos^2\beta$  and  $E_{\rm t} \approx \sin^2\beta$  with  $\beta = \nu\pi/2$ , which is valid if  $\Phi \leq \pi/2$  and  $-\infty < \operatorname{Im}\theta_{\pm} < -2$ . For  $-2 \leq \operatorname{Im}\theta_{\pm} < 0$  these can be improved by defining  $\beta$  as follows:

$$\tan^2 \beta = \tan^2 \left(\frac{\nu \pi}{2}\right) \tan \left[\nu \left(\frac{\pi}{2} + \theta\right)\right] \tan \left[\nu \left(\frac{\pi}{2} - \theta\right)\right]. \tag{33}$$

In contrast with the surface energy, the radiated energy  $E_{\rm d}$  achieves its maximum when  $\Phi=\pi$  and the wedge becomes an impedance half plane. The total energy flux  $E_{\rm s}+E_{\rm d}$ , as it might be expected from the energy balance (32), is invariant as the wedge angle changes, and always equals the energy flux  $E_{\rm i}$  of the incident wave, which is unity.

Finally, we note that the total field at the edge for an incident surface wave of unit amplitude is  $u_0(\pm \Phi \mp \theta_{\pm})$ , as it follows from definition (25). Based on the approximation  $E_s=1$  and the preceding discussion, and also using the representations (28)–(30) and assuming identical impedances with Re  $\theta=0$ , one may obtain the estimate

$$|u_0(\pm \Phi \mp \theta)| \approx v^{1/2} |\cot \theta|^{1/2}. \tag{34}$$

Referring to Fig. 4, we expect (34) to be accurate for wedge angle  $\Phi$  smaller than  $\pi/2$ .

## 2.3. The edge diffracted field

## 2.3.1. The diffraction coefficient

The diffraction integral (13) can be evaluated asymptotically for  $kr \gg 1$ , yielding the far-field asymptotic expression

$$u_{\rm d}(r,\phi) = D(\phi,\phi_0) \frac{\mathrm{e}^{\mathrm{i}(kr+\pi/4)}}{\sqrt{2\pi kr}} \{1 + \mathrm{O}[(kr)^{-1}]\},\tag{35}$$

where D, the diffraction coefficient, follows from the saddle point contributions to the integral at  $\alpha = \pm \pi$  as

$$D(\phi, \phi_0) = S(\phi - \pi) - S(\phi + \pi), \tag{36}$$

or, from Eq. (7) and (8)

$$D(\phi, \phi_0) = U_0 \frac{\nu \cos(\nu \phi_0)}{\Psi(\phi_0)} \left[ \frac{\Psi(\phi - \pi)}{\sin \nu (\phi - \pi) - \sin(\nu \phi_0)} - \frac{\Psi(\phi + \pi)}{\sin \nu (\phi + \pi) - \sin(\nu \phi_0)} \right]. \tag{37}$$

Using the property (23), we have

$$\Psi(\phi \pm \pi) = \frac{\psi_{\Phi}^{8}(\pi/2)}{\Psi(\phi)} \cos \left[\frac{\nu}{2} (\phi + \Phi \pm \theta_{+})\right] \cos \left[\frac{\nu}{2} (\phi + \Phi \pm \pi \mp \theta_{+})\right] \times \cos \left[\frac{\nu}{2} (\phi - \Phi \pm \theta_{-})\right] \cos \left[\frac{\nu}{2} (\phi - \Phi \pm \pi \mp \theta_{-})\right], \tag{38}$$

or with a bit of simplification,

$$\Psi(\phi \pm \pi) = \frac{\psi_{\phi}^{8}(\pi/2)}{4\Psi(\phi)} \left\{ \cos \left[ \nu \left( \frac{\pi}{2} - \theta_{+} \right) \right] - \sin \left[ \nu \left( \phi \pm \frac{\pi}{2} \right) \right] \right\} \times \left\{ \cos \left[ \nu \left( \frac{\pi}{2} - \theta_{-} \right) \right] + \sin \left[ \nu \left( \phi \pm \frac{\pi}{2} \right) \right] \right\}.$$
(39)

Substituting these into (37) yields, after some further algebra,

$$D(\phi, \phi_{0}) = U_{0} \frac{\nu}{4} \tan \left(\frac{\nu\pi}{2}\right) \psi_{\phi}^{8} \left(\frac{\pi}{2}\right) \frac{\cos(\nu\phi)}{\Psi(\phi)} \frac{\cos(\nu\phi_{0})}{\Psi(\phi_{0})} \times \left\{ 1 + \frac{\sin(\nu\phi) + \sin(\nu\phi_{0}) - 2\cos(\nu\pi/2)\cos\left[\nu(\pi/2 - \theta_{+})\right]}{\cos\left[\nu(\phi + \phi_{0})\right] + \cos\left(\nu\pi\right)} \times \frac{\sin(\nu\phi) + \sin(\nu\phi_{0}) + 2\cos\left(\nu\pi/2\right)\cos\left[\nu(\pi/2 - \theta_{-})\right]}{\cos\left[\nu(\phi - \phi_{0})\right] - \cos(\nu\pi)} \right\}.$$
(40)

Thus, using (25) and (26) we have the general result

$$D(\phi, \phi_0) = U_0 u_0(\phi) u_0(\phi_0) F_{\phi}(\phi, \phi_0), \tag{41}$$

where

$$F_{\phi}(\phi, \phi_{0}) = \frac{1}{4\nu} \tan\left(\frac{\nu\pi}{2}\right) \left\{ 1 + \frac{\sin(\nu\phi) + \sin(\nu\phi_{0}) - 2\cos(\nu\pi/2)\cos\left[\nu(\pi/2 - \theta_{+})\right]}{\cos\left[\nu(\phi + \phi_{0})\right] + \cos\left(\nu\pi\right)} \times \frac{\sin(\nu\phi) + \sin(\nu\phi_{0}) + 2\cos\left(\nu\pi/2\right)\cos\left[\nu(\pi/2 - \theta_{-})\right]}{\cos\left[\nu(\phi - \phi_{0})\right] - \cos(\nu\pi)} \right\}.$$
(42)

If the faces are purely reactive, i.e., the impedances and hence the angles  $\theta_{\pm}$  are all purely imaginary, then the magnitude of the edge field has the simple form [4]:

$$|u_0(\phi)| = \frac{2\nu \cos(\nu \phi)}{\left[\cosh(\nu |\theta_+|) - \sin(\nu \phi)\right]^{1/2} \left[\cosh(\nu |\theta_-|) + \sin(\nu \phi)\right]^{1/2}}.$$
(43)

Eqs. (41),(42) and (43) imply that the *magnitude* of the diffraction coefficient for a wedge with purely reactive faces can be found using trigonometric functions only. Determining the phase requires evaluating Malyuzhinets functions, in general.

Eqs. (41) and (42) clearly show that the diffraction coefficient is unchanged when the source and observation directions are reversed, i.e.,  $D(\phi_0, \phi) = D(\phi, \phi_0)$ , as required by the principle of reciprocity. In general, the diffracted response depends upon both the edge field  $u_0$  and the pattern function  $F_{\phi}$ . We have already discussed the behaviour of the former [4], and therefore we now need to consider only the pattern function  $F_{\phi}$ .

### 2.3.2. The pattern function $F_{\Phi}$

It is useful to consider some specific examples of the function  $F_{\Phi}$ . For the rigid wedge  $(\theta_{+} = \theta_{-} = 0)$ , we have  $u_{0}(\phi) = 2\nu$  and  $F_{\Phi} = F_{\Phi}^{R}$ , where

$$F_{\phi}^{R}(\phi,\phi_{0}) = \frac{1}{4\nu} \left[ \frac{\sin(\nu\pi)}{\cos(\nu\pi) - \cos[\nu(\phi - \phi_{0})]} + \frac{\sin(\nu\pi)}{\cos(\nu\pi) + \cos[\nu(\phi + \phi_{0})]} \right]. \tag{44}$$

This agrees with the well-known result for the rigid wedge, e.g. [14,29,30,36].

If the impedance is finite and  $\theta_+ = \theta_-$ , then

$$F_{\Phi}(\phi, \phi_0) = F_{\Phi}^{R}(\phi, \phi_0) + \frac{\sin(\nu \pi) \{\cos^2[\nu(\pi/2 - \theta_{\pm})] - \cos^2(\nu \pi/2)\}}{2\nu \{\cos(\nu \pi) + \cos[\nu(\phi + \phi_0)]\} \{\cos(\nu \pi) - \cos[\nu(\phi - \phi_0)]\}}.$$
(45)

Thus,  $F_{\Phi}$  and hence the diffraction coefficient vanishes for acute angles  $\Phi = \pi/2n$ ,  $n = 1, 2, 3, \ldots$ , if both faces have the same impedance. When the impedances are distinct the diffraction coefficient is zero for the subset of these angles with even n, i.e.,  $\Phi = \pi/4$ ,  $\pi/8$ ,  $\pi/16$ , etc., and this is in line with the general property found in Section 2. Other vertex angles of interest are  $\pi/2$  and  $\pi$ , corresponding to a half plane and a screen, respectively,

$$F_{\pi/2}(\phi, \phi_0) = \frac{1}{2} \frac{\sin \theta_+ - \sin \theta_-}{\sin \phi_+ + \sin \phi_0},\tag{46}$$

$$F_{\pi}(\phi, \phi_0) = \frac{1}{2} + \left[ \sin\left(\frac{\phi}{2}\right) + \sin\left(\frac{\phi_0}{2}\right) - \sqrt{2}\cos\left(\frac{\pi}{4} - \frac{\theta_+}{2}\right) \right] \times \frac{\sin(\phi/2) + \sin(\phi_0/2) + \sqrt{2}\cos(\pi/4 - \theta_-/2)}{\cos\phi + \cos\phi_0}. \tag{47}$$

The pattern function for a hard wedge (small  $\theta_{\pm}$ ) can be easily found. For instance, if the face impedances are identical and  $\theta_{\pm} = \theta$ , then (45) implies that

$$F_{\phi}(\phi,\phi_0) \approx F_{\phi}^{R}(\phi,\phi_0) \left[ 1 + \frac{\nu\theta \sin(\nu\pi)}{\cos(\nu\pi) - \sin(\nu\phi)\sin(\nu\phi_0)} \right]. \tag{48}$$

The case of a pressure-release wedge (u=0 on either face) is relevant to the problem of anti-plane shear wave diffraction in a clamped elastic wedge as well as electromagnetic diffraction of an E-polarised field by a perfectly conducting wedge. This limit can be found by letting  $\theta_{\pm} \to \pm i\infty$ . It is evident from (43) that the edge field vanishes,

while the pattern function  $F_{\Phi}$ , which is given by (42), becomes infinite, but the product in (41) remains finite and tends to the limit

$$D(\phi, \phi_0) = \nu U_0 \left[ \frac{\sin(\nu \pi)}{\cos(\nu \pi) - \cos\left[\nu(\phi - \phi_0)\right]} - \frac{\sin(\nu \pi)}{\cos(\nu \pi) + \cos\left[\nu(\phi + \phi_0)\right]} \right]. \tag{49}$$

This can be established by inserting into (36) the transform function relevant to the wedge with Dirichlet boundary conditions [29,36],

$$S(\alpha) = U_0 \frac{\nu \cos(\nu \phi_0)}{\sin(\nu \alpha) - \sin(\nu \phi_0)}.$$
 (50)

The pattern function  $F_{\Phi}(\phi, \phi_0)$  has singularities at the angular combinations which satisfy  $\cos(\nu\pi) \pm \cos\left[\nu(\phi \pm \phi_0)\right] = 0$ . Those corresponding to the shadow and reflection boundaries for acute wedges with  $\Phi > \pi/2(\nu < 1)$  occur at angles satisfying  $|\phi - \phi_0| = \pi$  and  $|\phi + \phi_0| = \pi/\nu - \pi$ . For obtuse wedges with  $\Phi < \pi/2(\nu > 1)$  the singularities are described as follows:

$$|\phi - \phi_0| = \frac{\pi}{\nu} (\tilde{\nu} + 1 - \nu), \quad |\phi + \phi_0| = \frac{\pi}{\nu} (\nu - \tilde{\nu}),$$
 (51)

where  $\tilde{v} = \text{entire}(v)$  and odd, and

$$|\phi - \phi_0| = \frac{\pi}{\nu} (\nu - \tilde{\nu}), \quad |\phi + \phi_0| = \frac{\pi}{\nu} (\tilde{\nu} + 1 - \nu),$$
 (52)

if  $\tilde{\nu}$  is even. All of these singularities can be interpreted in terms of geometrical optics constructions (see Section 2.1), and will not be discussed further here.

Based on these findings, and referring to (41) and (43), we conclude that to a very good approximation, the magnitude of the diffraction coefficient is

$$|D(\phi, \phi_0)| \approx U_0 \Omega(\phi) \Omega(\phi_0) |F_{\Phi}(\phi, \phi_0)|, \tag{53}$$

where

$$\Omega(\phi) = \frac{\nu \cos(\nu \phi)}{|\cos[(\nu/2)(\phi + \Phi - \theta_+)]\cos[(\nu/2)(\phi - \Phi + \theta_-)]|}$$

This is precise for reactive faces, and it provides a lower (upper) bound estimate when the faces have the same purely resistive impedance and  $\Phi > \pi/2(\Phi < \pi/2)$ .

## 2.3.3. The backscattering diffraction coefficient

We conclude Section 2 with a brief discussion of the backscattering properties of an impedance wedge. The backscattering diffraction coefficient results from (41) and (42) as

$$D(\phi, \phi) = \frac{U_0 u_0^2(\phi)}{2\nu \sin(\nu \pi)} \times \left\{ \sin^2 \left( \frac{\nu \pi}{2} \right) - \left[ \sin(\nu \phi) - \cos \left( \frac{\nu \pi}{2} \right) \cos \left( \nu \left( \frac{\pi}{2} - \theta_+ \right) \right) \right] \right.$$

$$\times \left. \frac{\sin(\nu \phi) + \cos(\nu \pi/2) \cos(\nu (\pi/2 - \theta_-))}{\sin^2(\nu \phi) - \cos^2(\nu \pi/2)} \right\}. \tag{54}$$

The monostatic backscattering echowidth  $\sigma$  normalised to the wavelength  $\lambda$  is defined in dB through the limit of the diffracted field [29]:

$$\frac{\sigma}{\lambda} = \lim_{r \to +\infty} 10 \lg_{10} \left( kr \frac{|u_{\rm d}(r,\phi)|^2}{|U_0|^2} \right),\tag{55}$$

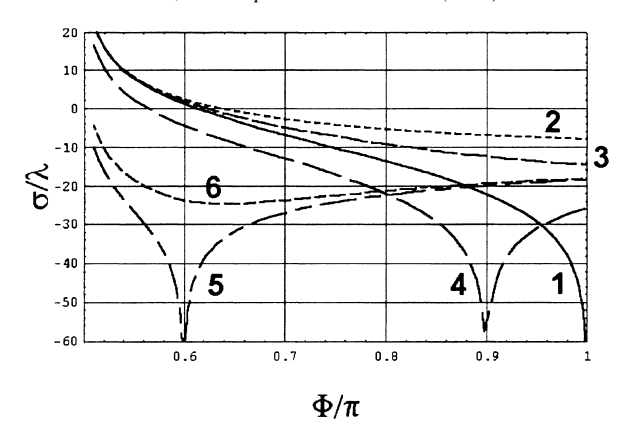


Fig. 5. The axial monostatic backscattering echowidth of an impedance wedge as a function of its vertex angle  $\Phi$ .

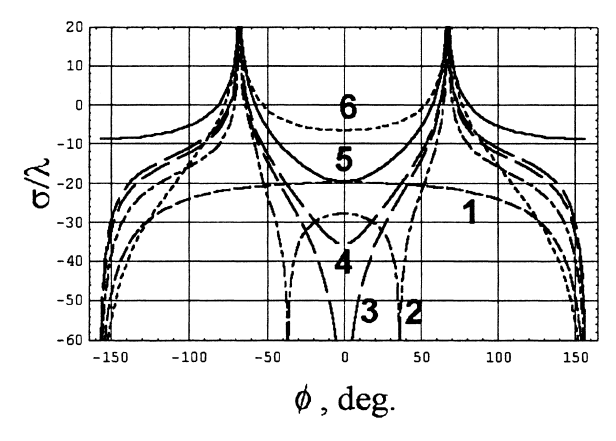


Fig. 6. The monostatic backscattering echowidth of an impedance wedge with  $\Phi = 7\pi/8$  as a function of the observation angle.

which on account of (35) gives

$$\frac{\sigma}{\lambda} = 20 \lg_{10} \left| \frac{D(\phi, \phi)}{\sqrt{2\pi} U_0} \right|. \tag{56}$$

Figs. 5 and 6 illustrate computational results characterising some important features of the monostatic backscattering echowidth of impedance wedges. Fig. 5 shows the echowidth in the axial direction ( $\phi = 0$  in (56)) as a function of the vertex angle  $\Phi$  for several values of the face impedances which we assume to be identical on both faces of the wedge, thus  $\theta_+ = \theta_- = \theta$ . The curves 1 and 2 correspond to the acoustically hard ( $\theta = 0$ ) and soft (Im  $\theta = \infty$ ) wedge, respectively, and they mark the extreme lines so that all other curves relevant to the intermediate values of the impedance with  $0 < |\text{Im}\theta| < +\infty$  lie between them (curve 3,  $\theta = -i$ ).

An interesting exception is the case of entirely real Brewster angles, illustrated by the curves 4 and 5. Note the presence of minima in those curves at the points defined by the relation  $\Phi + \theta = \pi$ . The cancellation of the backscattering echowidth follows from the representation (54) of the diffraction coefficient. One can readily check that the expression in parentheses vanishes when  $\Phi = \pi - \theta$  and  $\phi = 0$ . From the physical viewpoint this means that a wedge with a real value of its face impedance becomes "invisible" in the axial direction if its vertex angle  $\Phi$  satisfies this constraint. As the imaginary part of  $\theta$  grows, the minimum quickly disappears (curve 6,  $\theta = 2\pi/5 + 0.3i$ ). The numerical results given here for complex values of the Brewster angles  $\theta_{\pm}$  remain unchanged for complex conjugate quantities  $\bar{\theta}_{\pm}$  because of the property  $D(\phi, \phi_0, \bar{\theta}_+, \bar{\theta}_-) = \bar{D}(\phi, \phi_0, \theta_+, \theta_-)$  which is true as long as other parameters, i.e.,  $\phi$ ,  $\phi_0$ , and  $\Phi$  are real.

Fig. 6 shows how the monostatic backscattering echowidth of an impedance wedge of vertex angle  $\Phi=7\pi/8=157.5^{\circ}$  varies with the observation angle  $\phi$ . All curves in the figure are symmetric about the bisecting line  $\phi=0$  because the material properties of the wedge faces are assumed to be the same. Generally, no such symmetry exists when  $\theta_{+}\neq\theta_{-}$ . The maxima at  $\phi=\pm67.5^{\circ}$  correspond to the directions of specular reflection. The only case (curve 1) which remains bounded in those directions occurs when the normalised surface impedance is unity, or, equivalently,  $\theta=\pi/2$ , since in such an event the reflected wave vanishes at normal incidence. Curve 2 of Fig. 6, plotted for  $\theta=\pi/5$ , demonstrates that the phenomenon of the invisibility of an impedance wedge, mentioned before in the context of the axial backscattering  $\phi=0$ , may also take place at non-zero observation angles.

Simple analysis of the representation (54) shows that the zeros of the backscattering diffraction coefficient can be found from the relation

$$\sin^2(\nu\phi) = \cos(\nu\theta)\cos[\nu(\pi - \theta)]. \tag{57}$$

If  $\theta$  is entirely real and such that  $\pi - \Phi \le \theta \le \pi/2$ , then the equation has real-valued solutions for the observation angle  $\phi$  such that  $\nu|\phi| \le \arcsin{[\cos(\nu\pi/2)]}$ . Curve 3 in Fig. 6 corresponds to the intermediate case when  $\theta = \pi - \Phi$ , and there exists only one root of the above equation in the interval  $|\phi| \le \Phi$ . The backscattering diffraction coefficient loses this feature for smaller values of the Brewster angle (curve 4,  $\theta = \pi/10$ ), although the level of the echowidth in a sector around the central plane  $\phi = 0$  is still less than the one associated with the wedge with normalised surface impedance of unity ( $\theta = \pi/2$ , curve 1). The echowidth of a wedge with hard ( $\theta = 0$ , curve 5) or soft (Im  $\theta = \infty$ , curve 6) faces does not display any zeros, and the gap between those two extreme curves is monotonically filled with responses corresponding to finite values of the imaginary part of  $\theta$  (they are not shown in Fig. 6).

The examples in Figs. 5 and 6 indicate that the backscatter vanishes at particular observation angles  $\phi$  for a given wedge angle  $\Phi$  and surface impedance  $\theta$ . Conversely, the "invisibility" condition (57) can be solved for  $\theta$  in terms of  $\phi$  and  $\Phi$ :

$$\cos\left[\nu\left(\theta - \frac{\pi}{2}\right)\right] = \sqrt{\sin^2(\nu\phi) + \sin^2\left(\frac{\nu\pi}{2}\right)}.$$
 (58)

For  $\pi/2 \le \Phi \le \pi$ , as  $|\phi|$  goes from the forward direction  $\phi = 0$  to the boundary of the reflection zone  $|\phi| = \Phi - \pi/2$ , Eq. (58) on the interval  $0 \le \text{Re } \theta \le \pi/2$  has only one root

$$\theta = \frac{\pi}{2} - \frac{1}{\nu} \arccos\sqrt{\sin^2(\nu\phi) + \sin^2\left(\frac{\nu\pi}{2}\right)},\tag{59}$$

and the Brewster angle  $\theta$  increases from  $\pi - \Phi$  to  $\pi/2$ . The normalised surface admittance of the wedge faces is therefore

$$\sin \theta = \cos \left[ \frac{1}{\nu} \arccos \sqrt{\sin^2(\nu \phi) + \sin^2\left(\frac{\nu \pi}{2}\right)} \right],\tag{60}$$

which increases from  $\cos(\Phi - \pi/2)$  to 1. Within the reflection zone, as  $|\phi|$  is increased further to its maximum value  $|\phi| = \Phi$ , one gets two complex conjugate solutions of (58)

$$\theta = \frac{\pi}{2} \pm \frac{i}{\nu} \operatorname{arccosh} \sqrt{\sin^2(\nu\phi) + \sin^2\left(\frac{\nu\pi}{2}\right)},\tag{61}$$

which, however, lead to the same value of the parameter

$$\sin \theta = \cosh \left[ \frac{1}{\nu} \operatorname{arccosh} \sqrt{\sin^2(\nu \phi) + \sin^2\left(\frac{\nu \pi}{2}\right)} \right]. \tag{62}$$

This increases steadily with  $|\phi|$  to the value  $\cosh \{v^{-1} \operatorname{arcsinh}[\sin(v\pi/2)]\}$  for  $\phi = \pm \Phi$ . In summary, the backscattered edge diffraction in direction  $\phi$  vanishes if the surface impedance is real and given by (60) if  $0 \le |\phi| \le \Phi - \pi/2$ , and by (62) if  $\Phi - \pi/2 \le |\phi| \le \Phi$ .

# 3. Full uniform asymptotic expansions of the far-field

The diffraction coefficient  $D(\phi, \phi_0)$  plays a leading role in the far-field analysis of the diffraction by wedges. In fact, knowledge of the diffraction coefficient is the only information necessary to construct complete asymptotic representations of the scattered field for  $kr \gg 1$ . In this section we show how the representation (35), which includes only a major term of asymptotic expansion of the diffracted field in inverse powers of k and which as we saw above becomes infinite at shadow boundaries of incident and reflected waves, can be developed into a full asymptotic expansion of the total field which is bounded at all shadow boundaries and uniformly valid over the whole range of values of observation and incidence angles.

We start by deriving the higher order terms of the non-uniform representation (35). For simplicity we restrict the discussion to an exterior wedge, or  $\Phi > \pi/2$ . Assuming that no poles of the integrand in (13) lie near the saddle points  $\alpha = \pm \pi$ , the standard procedure for evaluating integrals over their steepest descent paths applies [30,37], yielding an expansion of the form

$$u_{\rm d}(r,\phi) \sim e^{\mathrm{i}kr} \sum_{n=0}^{+\infty} \left(\frac{\mathrm{i}}{kr}\right)^{n+1/2} A_n(\phi,\phi_0) \tag{63}$$

with the first term proportional to the diffraction coefficient,

$$A_0(\phi, \phi_0) = \frac{1}{\sqrt{2\pi}} D(\phi, \phi_0). \tag{64}$$

The higher-order coefficients  $A_n(\phi, \phi_0)$  with n = 1, 2, ..., are explicitly expressed through the zero-order coefficient by means of the relations

$$A_n(\phi, \phi_0) = \mathbf{Q}_n(\phi) A_0(\phi, \phi_0), \quad n = 1, 2, \dots,$$
 (65)

where  $\mathbf{Q}_n(\phi)$  are differential operators defined by

 $Q_0 = 1$ ,

$$\mathbf{Q}_n(\phi) = \frac{(-1)^n}{2^n n!} \left( \frac{\partial^2}{\partial \phi^2} + \frac{1}{4} \right) \left( \frac{\partial^2}{\partial \phi^2} + \frac{9}{4} \right) \dots \left( \frac{\partial^2}{\partial \phi^2} + \left( n - \frac{1}{2} \right)^2 \right). \tag{66}$$

These relations guarantee that (63) with arbitrary  $A_0(\phi, \phi_0)$  asymptotically satisfies the Helmholtz equation as  $kr \to \infty$ .

The representation (63) cannot be used when the observation point approaches shadow boundaries of the incident and reflected waves. Mathematically, this corresponds to the case in which certain poles of the integrand in (13) are in close proximity of the saddle points, and the conventional procedure for evaluating the SDP integrals are no longer applicable and should be appropriately corrected. Though such extensions of the saddle point technique are available (see, e.g., [30,37]), they are difficult to apply in diffraction problems if one is interested in finding a full uniform asymptotic expansion of the far-field rather than just the leading term. Here we adopt an elegant approach described by Borovikov and Kinber [14] who considered the particular case of a wedge with Dirichlet or Neumann boundary conditions. This allows us to avoid evaluating the integrals in (13) when the standard saddle point procedure fails, and it generalises the analysis of Borovikov and Kinber [14] to the arbitrary impedance wedge.

The algorithm for transforming the non-uniform expansion (63) into a uniform one is as follows. The discontinuous step functions in the ray optical part of the solution, which is given by (14), are replaced by Fresnel integrals of suitable arguments. It follows from its definition,

$$F(X) = \frac{e^{-i\pi/4}}{\sqrt{\pi}} \int_{-\infty}^{X} e^{is^2} ds,$$
(67)

that the Fresnel integral F(X) is a smooth function of its argument. As  $X \to \pm \infty$  it tends to the step function H(X), which is evident from the asymptotic representation

$$F(X) \sim H(X) + \frac{e^{iX^2 - i3\pi/4}}{2\pi X} \sum_{n=0}^{+\infty} \frac{\Gamma(n + \frac{1}{2})}{(iX^2)^n},$$
(68)

with  $\Gamma(z)$  being the gamma function.

In order to recover the non-uniform formulas outside the immediate vicinity of the shadow boundary the argument of a Fresnel integral in a uniform representation is chosen as  $X = \sqrt{k(s_{\rm d} - s_{\rm go})}$  where  $s_{\rm d} = r$  is the eikonal of the edge-diffracted wave and  $s_{\rm go}$  is the eikonal of the ray associated with a given shadow boundary. This latter eikonal is given by  $s_{\rm go} = -r\cos(\phi - \phi_0)$  for the incident plane wave and by  $s_{\rm go} = -r\cos(\phi + \phi_0 \mp 2\Phi)$  for plane waves reflected from upper and lower wedge faces. At the shadow boundary  $s_{\rm d} = s_{\rm go}$ . Outside the shadow boundary the sign of the square root function in the argument of the Fresnel integral is defined to be positive on the lit side and negative on the shadowed side. Eq. (68) then ensures that the correct field structure is recovered at observation points distant from the penumbra region.

One may check that  $e^{iks_{go}}F\left[\sqrt{k(s_d-s_{go})}\right]$  exactly satisfies the Helmholtz equation by direct substitution into (2). Correspondingly, the edge-diffracted term in the uniform representation independently satisfies the Helmholtz equation. We assume that the edge-diffracted field is of the form of expansion (63) with coefficients  $A_n$ ,  $n=1,2,\ldots$ , given by the recurrence relations (65). However, the zero-order coefficient differs from  $A_0(\phi,\phi_0)$  of (64), but is determined by requiring that the uniform and non-uniform representations reduce to each other outside the penumbra region. This is achieved by expanding the Fresnel integral according to (68), and equating terms of order  $(kr)^{-1/2}$ .

In what follows we distinguish four specific cases, in accordance with the structure of the ray optical field.

(a) The incident field illuminates only the lower face of the wedge ( $-\Phi < \phi_0 < \Phi - \pi$ ). In this case there are two shadow boundaries at  $\phi = \phi_0 + \pi$  and  $\phi = \pi - 2\Phi - \phi_0$  associated with the incident wave and the wave reflected from the lower face of the wedge. Applying the procedure described above leads to the far-field representation of the form (12) with the geometric optic and diffracted contributions corrected as follows:

$$u_{g}(r,\phi) = U_{0}F\left[\sqrt{2kr}\cos\left(\frac{\phi - \phi_{0}}{2}\right)\right]e^{-ikr\cos(\phi - \phi_{0})} + U_{0}R_{-}(\Phi + \phi_{0})F\left[\sqrt{2kr}\cos\left(\frac{\phi + \phi_{0} + 2\Phi}{2}\right)\right]e^{-ikr\cos(\phi + \phi_{0} + 2\Phi)},$$
(69)

$$u_{\rm d}(r,\phi) \sim e^{ikr} \sum_{n=0}^{+\infty} \left(\frac{i}{kr}\right)^{n+1/2} B_n(\phi,\phi_0),$$
 (70)

$$B_0(\phi, \phi_0) = \frac{1}{\sqrt{2\pi}} D(\phi, \phi_0) + \frac{1}{2\sqrt{2\pi} \cos((\phi - \phi_0)/2)} + \frac{R_-(\phi + \phi_0)}{2\sqrt{2\pi} \cos((\phi + \phi_0 + 2\phi)/2)},$$
(71)

$$B_n(\phi, \phi_0) = \mathbf{Q}_n(\phi)B_0(\phi, \phi_0), \quad n = 1, 2, \dots$$
 (72)

Here,  $R_{-}(\Phi + \phi_0)$  is the reflection coefficient introduced in (15).

One may verify that the two expressions (69) and (70) independently satisfy the Helmholtz equation. The zero-order coefficient  $B_0(\phi, \phi_0)$  given by (71) is a bounded and analytic function of  $\phi$  at shadow boundaries  $\phi = \phi_0 + \pi$ 

and  $\phi = \pi - 2\Phi - \phi_0$  because the poles of the diffraction coefficient  $D(\phi, \phi_0)$  at those points are cancelled by other members of (71). The higher-order coefficients  $B_n(\phi, \phi_0)$  with n = 1, 2, ..., defined by (72) are also analytic at the shadow boundaries because they are obtained by differentiation of the analytical function  $B_0(\phi, \phi_0)$ . The representation (12), combined with Eqs. (69),(70) and (71), is therefore valid for arbitrary location of the observation point, provided that the excitation conforms with the requirement  $-\Phi < \phi_0 < \Phi - \pi$ . Away from the shadow boundaries the Fresnel integrals in (69) can be replaced by their asymptotic representation (68), which converts the uniform formulas into the non-uniform ones with  $u_g(r, \phi)$  and  $u_d(r, \phi)$  given by (14) and (63).

(b) Both faces of the wedge are illuminated by the incident field  $(\Phi - \pi < \phi_0 < \pi - \Phi)$ . In this event there are two shadow boundaries at  $\phi = \pm 2\Phi \mp \pi - \phi_0$ , associated with the fields reflected from the wedge faces, while the direct wave is omnipresent. The geometrical optics part of (12) is then

$$u_{g}(r,\phi) = U_{0}e^{-ikr\cos(\phi - \phi_{0})} + U_{0}R_{+}(\Phi - \phi_{0})F\left[\sqrt{2kr}\cos\left(\frac{\phi + \phi_{0} - 2\Phi}{2}\right)\right]e^{-ikr\cos(\phi + \phi_{0} - 2\Phi)} + U_{0}R_{-}(\Phi + \phi_{0})F\left[\sqrt{2kr}\cos\left(\frac{\phi + \phi_{0} + 2\Phi}{2}\right)\right]e^{-ikr\cos(\phi + \phi_{0} + 2\Phi)}.$$
(73)

The expansion of the diffracted component  $u_d(r, \phi)$  is of the same form as in (70) and (72), except for the zero-order coefficient

$$B_0(\phi, \phi_0) = \frac{1}{\sqrt{2\pi}} D(\phi, \phi_0) + \frac{R_+(\Phi - \phi_0)}{2\sqrt{2\pi} \cos((\phi + \phi_0 - 2\Phi)/2)} + \frac{R_-(\Phi + \phi_0)}{2\sqrt{2\pi} \cos((\phi + \phi_0 + 2\Phi)/2)},$$
 (74)

which in this case should be continuous at  $\phi = \pm 2\Phi \mp \pi - \phi_0$ . Away from these directions the expressions (73) and (74) reduce to the non-uniform formulas.

(c) The incident field illuminates the upper face of the wedge  $(\pi - \Phi < \phi_0 < \Phi)$ . Now, instead of (69),(71),(73) and (74), we have

$$u_{g}(r,\phi) = U_{0}F\left[\sqrt{2kr}\cos\left(\frac{\phi - \phi_{0}}{2}\right)\right]e^{-ikr\cos(\phi - \phi_{0})} + U_{0}R_{+}(\Phi - \phi_{0})F\left[\sqrt{2kr}\cos\left(\frac{\phi + \phi_{0} - 2\Phi}{2}\right)\right]e^{-ikr\cos(\phi + \phi_{0} - 2\Phi)},$$

$$(75)$$

$$B_0(\phi, \phi_0) = \frac{1}{\sqrt{2\pi}} D(\phi, \phi_0) + \frac{R_+(\Phi - \phi_0)}{2\sqrt{2\pi} \cos((\phi + \phi_0 - 2\Phi)/2)} + \frac{1}{2\sqrt{2\pi} \cos((\phi - \phi_0)/2)},$$
(76)

which is uniformly valid outside the wedge, including the shadow boundaries  $\phi = \phi_0 - \pi$  and  $\phi = 2\Phi - \pi - \phi_0$ . (76) is consistent with (14) and (63) outside the penumbra regions (75).

(d) The intermediate case ( $\phi_0 \approx \pm \pi \mp \Phi$ ). The uniform formulas given above become inapplicable in this case because they are not uniform as functions of the incidence angle  $\phi_0$  and, therefore, do not provide a continuous transition from case (a) to (b) and from (b) to (c). The required extension is given by the formulas

$$u_{g}(r,\phi) = U_{0}F\left[\sqrt{2kr}\cos\left(\frac{\phi - \phi_{0}}{2}\right)\right]e^{-ikr\cos(\phi - \phi_{0})} + U_{0}R_{+}(\Phi - \phi_{0})F\left[\sqrt{2kr}\cos\left(\frac{\phi + \phi_{0} - 2\Phi}{2}\right)\right] \times e^{-ikr\cos(\phi + \phi_{0} - 2\Phi)} + U_{0}R_{-}(\Phi + \phi_{0})F\left[\sqrt{2kr}\cos\left(\frac{\phi + \phi_{0} + 2\Phi}{2}\right)\right]e^{-ikr\cos(\phi + \phi_{0} + 2\Phi)}, \quad (77)$$

$$u_{\rm d}(r,\phi_0) \sim U_0 \,\mathrm{e}^{\mathrm{i}kr} \sum_{n=0}^{+\infty} \left(\frac{\mathrm{i}}{kr}\right)^{n+1/2} C_n(\phi,\phi_0),$$
 (78)

$$C_{0}(\phi, \phi_{0}) = \frac{1}{\sqrt{2\pi}} D(\phi, \phi_{0}) + \frac{1}{2\sqrt{2\pi} \cos((\phi - \phi_{0})/2)} + \frac{R_{+}(\Phi - \phi_{0})}{2\sqrt{2\pi} \cos((\phi + \phi_{0} - 2\Phi)/2)} + \frac{R_{-}(\Phi + \phi_{0})}{2\sqrt{2\pi} \cos((\phi + \phi_{0} + 2\Phi)/2)},$$

$$(79)$$

$$C_n(\phi, \phi_0) = \mathbf{Q}_n(\phi)C_0(\phi, \phi_0), \quad n = 1, 2, \dots$$
 (80)

One may check that  $C_0(\phi, \phi_0)$  is an analytic function of  $\phi$  at each of the four shadow boundaries  $\phi = \phi_0 \pm \pi$ ,  $\phi = \pm 2\Phi \mp \pi - \phi_0$ , and so are the higher-order coefficients  $C_n(\phi, \phi_0)$  with n = 1, 2, ... As the incident angle  $\phi_0$  moves away from an immediate vicinity of the directions  $\phi_0 = \pm \pi \mp \Phi$ , we may replace one of the three Fresnel integrals in (77) with its asymptotic expansion (68), which transforms case (d) into one of the cases (a), (b), or (c). When the observation point is sufficiently far from all shadow boundaries, further simplifications are achieved by replacing all remaining Fresnel integrals in (77) with their asymptotic representations, which converts the formulas (77),(78) and (79) into (14),(63),(64) and (65).

We note that the task of finding the correct representation for case (d) by means of traditional technique would require the evaluation of the diffraction integral (13) in the limit as three poles simultaneously approach the saddle point.

Other singularities of the transform function  $S(\alpha + \phi)$  can occur close to the saddle points in the diffraction integral (13). Specifically, these are the poles associated with the surface waves. When  $|\theta_{\pm}| \ll 1$ , some new transition regions may exist near the wedge faces, which should be accounted for in the far-field representation. This case does not produce any crucial difficulties and can be treated using conventional tools of diffraction theory (see, e.g., [32]).

We are now ready to consider how the field diffracted by an impedance wedge is distributed in space. Fig. 7 shows the angular distribution of the total field amplitude  $|u(r,\phi)|$  at a distance  $r=1.6\lambda$  from the edge of a wedge with  $\Phi=7\pi/8=157.5^{\circ}$ , assuming the plane wave excitation (1) with  $U_0=1$  and  $\phi_0=\pi/2$ . The solid line corresponds to the limiting case of acoustically hard faces  $\theta_{\pm}=0$ , whereas the dotted one relates to soft boundaries with Im  $\theta_{\pm}\to\infty$ . Clearly distinguished in the plot are the shadow region  $(-157.5^{\circ}<\phi<-90^{\circ})$ , the intermediate region illuminated only by the incident wave  $(-90^{\circ}<\phi<45^{\circ})$ , and the region where both incident and reflected waves are present  $(45^{\circ}<\phi<157.5^{\circ})$ . The oscillations in the curves within the intermediate zone arise from the superposition of the incident and edge-diffracted fields. For  $\phi>45^{\circ}$  the wave reflected from the upper boundary also contributes, resulting in stronger fluctuations of the total field.

The field diffracted by a wedge with face impedance equal to unity ( $\theta_{\pm} = \pi/2$ , the dashed line in Fig. 7) displays relatively weak oscillations because of the small reflected amplitude. The diffracted component is also of lower amplitude, which is evident by comparison of the curves in the intermediate zone.

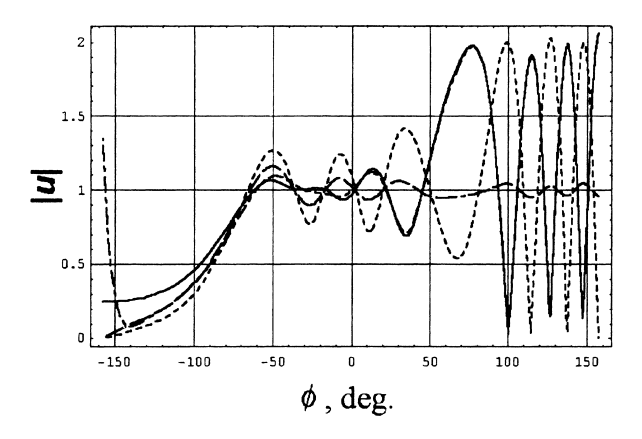


Fig. 7. Total field due to plane wave excitation at kr = 10 from the edge of an impedance wedge.

The dot-dashed curve ( $\theta_+ = 0$  and  $\theta_- = -i$ ) illustrates the case in which a surface wave propagates over the shadowed face of the wedge. The surface wave may become the main contribution to the total field near a face with finite impedance. As the observation point moves outward from the wedge face, the amplitude of the surface wave rapidly decreases dropping below the level of the ordinary shadow field. This can be seen from the dot-dashed curve, which almost coincides with other curves outside an immediate vicinity of the wedge face.

#### 4. Conclusions

A complete analysis of the far-field diffraction by an arbitrarily angled wedge with arbitrary face impedance has been presented. Both plane and surface wave excitation have been considered.

Scattering and radiation of an incident surface wave from the edge of an impedance wedge have been analysed using accurate representations for the transmission, reflection, and radiation coefficients. Simple approximate formulas have been found which permit accurate estimates of the magnitudes of the surface wave reflection and transmission coefficients.

A full asymptotic representation of the far-field diffracted by an impedance wedge has been deduced which remains uniformly valid for arbitrary incidence and observation directions. Explicit formulae are given for the uniformly asymptotic far-field of an exterior wedge ( $\Phi > \pi/2$ ).

The tip amplitude  $u_0$  has been shown to be intimately involved in the far-field diffraction coefficient  $D(\phi, \phi_0)$ . The only additional quantity required for the latter is a pattern function which comprises trigonometric functions only. The remarkably simple factorisation,  $D(\phi, \phi_0) = u_0(\phi)u_0(\phi_0)F_{\phi}(\phi, \phi_0)$ , derived here for the first time, is convenient for approximating and bounding the diffraction from impedance boundaries, and leads to exact results for purely reactive faces. The simplicity of the pattern function,  $F_{\phi}$ , allows one to choose the surface impedance to meet specific criteria. For example, the far-field backscatter for head-on incidence vanishes if both faces have real impedance such that  $\theta = \pi - \Phi$ . The concept of choosing the material properties to eliminate edge diffraction generalises the common practice of impedance matching between two half spaces in order to eliminate reflection. This is a new idea, which is made feasible by the explicit factorisation of D.

## Acknowledgements

The work of A.N. Norris was supported by the Office of Naval Research.

## References

- [1] G.D. Malyuzhinets, Generalisation of the Reflection Method in the Theory of Diffraction of Sinusoidal Waves (Doctoral dissertation, P.N. Lebedev Phys. Inst. Acad. Sci. USSR, 1950), in Russian.
- [2] G.D. Malyuzhinets, The principle of extinction and the problem of stimulated vibrations in an arbitrary domain, Zh. Tech. Fiziki 21 (1951) 881–885 (in Russian).
- [3] G.D. Malyuzhinets, Excitation, reflection and emission of surface waves from a wedge with given face impedances, Sov. Phys. Dokl. 3 (1958) 752–755.
- [4] A.V. Osipov, A.N. Norris, The Malyuzhinets theory for scattering from wedge boundaries: A review, Wave motion 29 (1999) 313-340.
- [5] W.E. Williams, Diffraction of an E-polarised plane wave by an imperfectly conducting wedge, Proc. R. Soc. London A 252 (1959) 376–393.
- [6] T.B.A. Senior, Diffraction by an imperfectly conducting wedge, Commun. Pure Appl. Math. 12 (1959) 337–372.
- [7] G.L. James, Uniform diffraction coefficients for an impedance wedge, Electron. Lett. 13(14) (1977) 403-404.
- [8] R. Tiberio, G. Pelosi, G. Manara, A uniform GTD formulation for the diffraction by a wedge with impedance faces, IEEE Trans. Antennas Propagat. 33 (1985) 867–873.
- [9] M.P. Zavadskaya, R.P. Starovoitova, Edge waves in G.D. Malyuzhinets' solution for an impedance wedge, Sov. Phys. Acoust. 34 (1988) 678–680
- [10] G. Pelosi, S. Maci, R. Tiberio, A. Michaeli, Incremental length diffraction coefficients for an impedance wedge, IEEE Trans. Antennas Propagat. 40 (1992) 1201–1210.

- [11] J.B. Keller, Geometrical theory of diffraction, J. Opt. Soc. Am. 52 (1962) 116-130.
- [12] D.S. Ahluwalia, R.M. Lewis, J. Boersma, Uniform asymptotic theory of diffraction by a plane screen, SIAM J. Appl. Math. 16 (1968) 783–807.
- [13] S.W. Lee, G.A. Deshamps, A uniform asymptotic theory of EM diffraction by a curved wedge, IEEE Trans. Antennas Propagat. 24 (1976)
- [14] V.A. Borovikov, B.Ye. Kinber, Geometrical Theory of Diffraction, IEE Electromagnetic Waves Series, no. 37, London, 1994.
- [15] R.G. Kouyoumjian, P.H. Pathak, A uniform geometrical theory of diffraction for an edge in a perfectly conducting surface, Proc. IEEE 62 (1974) 1448–1461.
- [16] P.Ya. Ufimtsev, Method of edge waves in the physical theory of diffraction U.S. Air Force Systems Command Foreign Technology Office Document ID No. FTD-HC-23-259-71 (1971), translation of Russian original.
- [17] K.M. Mitzner, Incremental length diffraction coefficients, Aircraft Division Northrop Corporation Technical Report No. AFAL-TR-73-296 (1974).
- [18] R.A. Shore, A.D. Yaghjian, Incremental diffraction coefficients for planar surfaces, IEEE Trans. Antennas Propagat. 36 (1988) 55-70.
- [19] R. Tiberio, S. Maci, A. Toccafondi, An incremental theory of diffraction: electromagnetic formulation, IEEE Trans. Antennas Propagat. 43 (1995) 89–96.
- [20] C.E. Ryan, L. Peters Jr., Evaluation of edge-diffracted fields including equivalent currents for the caustic regions, IEEE Trans. Antennas Propagat. 17 (1969) 292–299.
- [21] A. Michaeli, Equivalent edge currents for arbitrary aspects of observation, IEEE Trans. Antennas Propagat. 32 (1984) 252–258.
- [22] A. Michaeli, Elimination of infinities in equivalent edge currents, Part I: Fringe current components, IEEE Trans. Antennas Propagat. 34 (1986) 912–918.
- [23] A. Michaeli, Elimination of infinities in equivalent edge currents, Part II: Physical optics components, IEEE Trans. Antennas Propagat. 34 (1986) 1034–1037.
- [24] D.I. Butorin, P.Ya. Ufimtsev, Explicit expressions for an acoustic edge wave scattered by an infinitesimal edge element, Sov. Phys. Acoust. 32 (1986) 283–287.
- [25] P.Y. Ufimtsev, Elementary edge wave and the physical theory of diffraction, Electromagnetics 11 (1991) 125–159.
- [26] A.F. Filippov, Investigation of solution of a nonstationary problem of diffraction of a plane wave by an impedance wedge, Zh. Vych. Matem. i Mat. Fiziki 7 (1967) 825-835, in Russian.
- [27] J. Boersma, Y. Rahmat-Samii, Comparison of two leading uniform theories of edge diffraction with the exact uniform asymptotic solution, Radio Sci. 15 (1980) 1179–1194.
- [28] A.D. Pierce, W.J. Hadden Jr., Plane wave diffraction by a wedge with finite impedance, J. Acoust. Soc. Am. 63 (1978) 17–27.
- [29] J.J. Bowman, T.B.A. Senior, The wedge, in: J.J. Bowman, T.B.A., P.L.E. Uslenghi (Eds.), Electromagnetic and Acoustic Scattering by Simple Shapes, North-Holland, Amsterdam, 1969, pp. 252–283.
- [30] L.B. Felsen, N. Marcuvitz, Radiation and Scattering of Waves, Prentice-Hall, New York, 1978.
- [31] T. Griesser, C.A. Balanis, Reflections, diffractions, and surface waves for an interior impedance wedge of arbitrary angle, IEEE Trans. Antennas Propagat. 37 (1989) 927–935.
- [32] A.V. Osipov, Uniform asymptotic formula for calculating an acoustic field near a face of an impedance wedge, Sov. Phys. Acoust. 36 (1990) 180–183.
- [33] A.V. Osipov, Asymptotic representation of the sound field in a narrow angular region with impedance boundaries, Sov. Phys. Acoust. 36 (1990) 287–290.
- [34] A. Sommerfeld, Optik, Vorlesungen über Theoretische Physik, Bd. 4, Geest & Portig, Leipzig, BRD, 1959.
- [35] A. Sommerfeld, Theorie der beugung, in: P. Frank, R.V. Mises (Eds.), Die Differential und Integralgleichungen der Mechanics und Physics, Bd. 2, Vieweg and Son, Braunschweig, BRD, 1961.
- [36] A.D. Pierce, Acoustics: An Introduction to its Physical Principles and Applications, Acoustical Society of America, Woodbury, NY, 1989.
- [37] F.W.J. Olver, Asymptotics and Special Functions, Academic Press, New York, 1974.